Hindawi
International Journal of Antennas and Propagation
Volume 2018, Article ID 8629806, 8 pages
https://doi.org/10.1155/2018/8629806

Research Article

Detection of Subsurface Target Based on FDA-MIMO Radar

Qinghua Liu,[1,2] **Chang Jiang**,[1,3] **Liangnian Jin**,[1,3] **and Shan Ouyang**[1,3]

[1]*School of Information and Communication, Guilin University of Electronic Technology, Guilin 541004, China*
[2]*Science and Technology on Near-Surface Detection Laboratory, Wuxi 214035, China*
[3]*Guangxi Key Lab of Wireless Wideband Communication and Signal Processing, Guilin University of Electronic Technology, Guilin 541004, China*

Correspondence should be addressed to Qinghua Liu; liuqinghuagl@126.com

Received 4 August 2018; Accepted 2 October 2018; Published 23 December 2018

Academic Editor: Ana Alejos

As a new type of radar, the FDA-MIMO radar has a good improvement on side lobe suppression and target detection performance compared with the conventional MIMO radar. However, the existing researches on FDA-MIMO radar are almost based on far-field. In this paper, FDA-MIMO radar is applied to the detection of subsurface targets. Aimed at near-subsurface targets, we formulated the signal model of FDA-MIMO radar and combined it with the algorithm of grid of beam (GOB) to detect. Compared with conventional MIMO radar detection, we verified the effectiveness of the proposed method through theoretical simulation.

1. Introduction

Detecting underground targets is of great importance both in military and civilian applications. Ground penetrating radar (GPR) [1–4] detection is the most commonly employed approach for underground target detection. It emits electromagnetic signals by transmitting antennas and receives echoes from targets by receiving antennas. For a long time, single-input single-output (SISO) was used to detect targets in most of the traditional ground penetrating radar systems, which uses one antenna to emit electromagnetic signals and uses one antenna to receive echoes. Although SISO radar has the advantages of simple system and convenient detection, its detection performance is difficult to get greater improvement because of the limited amount of information it acquires [5]. With the development of radar technology and the steady increase of application requirements, multiple-input multiple-output (MIMO) radar has received wide attention [6–9]. It employs multiple antennas to emit orthogonal waveforms or noncoherent waveforms and multiple antennas to receive the echoes reflected by the targets. Compared with the SISO radar system, the MIMO radar system makes use of the spatiotemporal information of the targets more effectively, which makes it not only have better performance of target parameter estimation but also stronger anti-interference ability and imaging resolution, and the detection performance has been improved qualitatively.

Since the frequency diverse array [10, 11] was first proposed by Antonik et al. in 2006, many scholars from all over the world have conducted research on it. Different from traditional phased array, FDA introduces a small frequency increment across the array elements [12, 13], which induces the beam pattern curved in space that extends the spatial degrees of freedom. In [14], FDA was applied to the detection of ground moving targets in forward-looking radar. Compared with traditional phased array radar, it can suppress the range ambiguity clutter to a certain extent. In [15], FDA was first applied to synthetic aperture radar for high-resolution imaging. It was verified by simulation that FDA can improve the imaging resolution of azimuth direction and range direction of synthetic aperture radar. In [16], Sammartino et al. combined FDA and MIMO radar technology for the first time and proposed the concept of MIMO radar with frequency and waveform diversity. The FDA-MIMO radar combines the advantages of FDA radar and MIMO radar. It not only obtains the excellent target detection performance of the MIMO radar but also possesses the

spatial degree of freedom of the FDA radar. On this basis, the specific application of the FDA-MIMO radar was further studied in [17, 18], and it was concluded that the FDA-MIMO radar has a good improvement on side lobe suppression and target detection performance. FDA and waveform multiplexing have been applied to bistatic radar systems in [19]. The effect of frequency increment error on the adaptive beamforming and target detection performance of FDA-MIMO radar has been studied in detail in [20], which provides theoretical guidance for the design of FDA-MIMO radar. It is worth noting that the existing researches on FDA are almost based on far-field.

In this paper, FDA-MIMO radar is applied to the detection of near-subsurface targets. Different from most researches on FDA which are based on far-field, we formulated the signal model of FDA-MIMO radar based on near-subsurface target detection, and we chose the appropriate array spacing which is better for GPR application. Due to the difference in propagation media between most researches in free space and our research under the ground, we set the frequency increment which is more appropriate for this study. We achieved the target location by GOB algorithm through theoretical simulation. Compared with conventional MIMO radar, its detection effect has been improved.

The rest of this paper is organized as follows. Section 2 is the modeling part. We formulate the signal model of the transmitter and receiver of the FDA-MIMO radar and analyze the model combining with near-subsurface targets. Section 3 is the data processing part. We separate the echo signals after receiving, then process the echo data through algorithm and output the simulation results by 2D images. Section 4 is the experimental simulation and analysis part. We perform the theoretical simulation according to the data processing method in Section 3 and compare the simulation results with conventional MIMO radar. Finally, conclusions are drawn in Section 5.

2. Signal Model of FDA-MIMO Radar

In this section, we consider the signal model of the FDA-MIMO radar, as shown in Figure 1. The FDA-MIMO radar includes N transmitting antennas and N receiving antennas. MF stands for the matched filter in the receiver. Different from conventional MIMO radar whose transmitting array element transmits the same carrier frequency signal; FDA-MIMO radar uses a small frequency increment across its transmitting array elements. We use FDA to transmit signals that the carrier frequency increased linearly between adjacent array elements. The radiated signal frequency of each transmitting array element is as follows:

$$f_n = f_0 + (n-1)\Delta f, \quad n = 1, 2, \ldots, N, \tag{1}$$

where f_n is the radiation frequency of the nth element, f_0 is the FDA operating carrier frequency, Δf is the frequency increment, and N is the number of transmitting array elements.

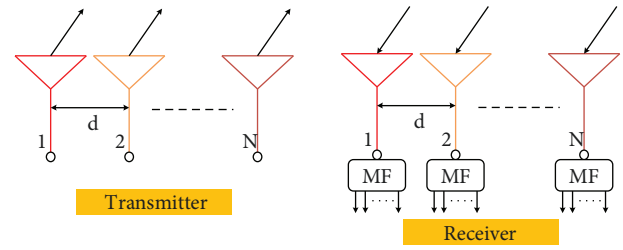

Figure 1: Illustration of FDA-MIMO radar system.

The FDA-MIMO radar emits narrow band signals. Due to the slow fluctuation of signal envelope under narrow band condition, the complex envelope of signal can be regarded as a constant. The signal transmitted by the nth array element can be approximately represented as a complex exponential function and is formulated as follows:

$$s_n(t) = \exp\{j2\pi f_n t\}. \tag{2}$$

The signals emitted by the transmitting arrays are received by the receiving arrays after being reflected by the targets. The signal received by the mth receiving element can be represented by the following:

$$y_m(t) = \beta \sum_{n=1}^{N} \exp\{j2\pi f_n (t - \tau_{n,m})\} + n_m(t), \tag{3}$$

where β is the reflection coefficient of the target, $\tau_{n,m}$ is the signal propagation time from the nth transmitting element to the mth receiving element, $n_m(t)$ is the noise received by the mth receiving element. Combined with the near-subsurface target, the model of GPR based on FDA-MIMO is shown in Figure 2.

We set the first element as reference element. p is a near-subsurface target, located at (X_p, Z_p). X_p and Z_p are the horizontal and vertical distances between the target p and the reference element, respectively. We consider the FDA-MIMO radar with uniform linear array (ULA). The transceiver antenna that uses the same antenna to transmit and receive electromagnetic signals is applied to FDA-MIMO radar. The distance between the adjacent antenna elements is d. According to the geometric relation, the distance from the nth transmitting element to the target p is the following:

$$r_n = \sqrt{X_p^2 + Z_p^2 + ((n-1)d)^2 - 2(n-1)dX_p}. \tag{4}$$

Since the FDA-MIMO radar uses transceiver antenna, the distance from the target p to the mth receiving element is as follows:

$$r_m = \sqrt{X_p^2 + Z_p^2 + ((m-1)d)^2 - 2(m-1)dX_p}. \tag{5}$$

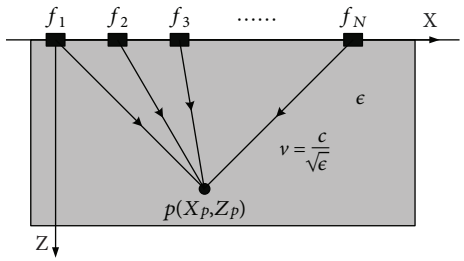

Figure 2: Model of GPR based on FDA-MIMO.

Thus, the signal propagation time from the nth transmitting element to the mth receiving element is as follows:

$$\tau_{n,m} = \frac{\sqrt{X_p^2 + Z_p^2 + ((n-1)d)^2 - 2(n-1)dX_p}}{v} + \frac{\sqrt{X_p^2 + Z_p^2 + ((m-1)d)^2 - 2(m-1)dX_p}}{v}, \tag{6}$$

where v represents the propagation speed of electromagnetic waves in the underground medium, which is related to the relative dielectric constant of underground medium. The specific expression is as follows:

$$v = \frac{c}{\sqrt{\varepsilon}}, \tag{7}$$

where c represents the propagation speed of electromagnetic waves in a vacuum and ε represents the relative dielectric constant of the underground medium. According to the signal propagation time, the signal received by the mth element can be represented by

$$y_m(t) = \beta_p \sum_{n=1}^{N} \exp\left\{ j2\pi f_n \cdot \left(t - \frac{\sqrt{X_p^2 + Z_p^2 + ((n-1)d)^2 - 2(n-1)dX_p}}{v} - \frac{\sqrt{X_p^2 + Z_p^2 + ((m-1)d)^2 - 2(m-1)dX_p}}{v} \right) \right\} + n_m(t), \tag{8}$$

where β_p is the reflection coefficient of the target p, $n = 1, 2, \ldots, N$, and $m = 1, 2, \ldots, N$.

3. Data Processing of FDA-MIMO Radar

3.1. Signal Separation in the Receiving End. Each receiving element of the FDA-MIMO radar is connected to a matched filter bank to demodulate the echo signals. In the receiver, the signals are downconverted to baseband first and then separated by matched filter. The matched filtering output in the mth receiving element for the nth transmitting element is as follows:

$$y_{n,m}(X_p, Z_p) = \beta_p \exp\left\{ j2\pi(f_0 + (n-1)\Delta f) \cdot \left(- \frac{\sqrt{X_p^2 + Z_p^2 + ((n-1)d)^2 - 2(n-1)dX_p}}{v} - \frac{\sqrt{X_p^2 + Z_p^2 + ((m-1)d)^2 - 2(m-1)dX_p}}{v} \right) \right\} + n_{n,m}(t). \tag{9}$$

3.2. Algorithm Processing. We use the idea of the gird of beam algorithm from beamforming technology to scan and output the echo signals. FDA-MIMO radar equipped with N transmitting elements and N receiving elements, so each group of echo signals after demodulation through the matched filter bank can obtain $N \times N$ echo data. We represent these $N \times N$ echo data in vector form as follows:

$$\boldsymbol{y}(X_p, Z_p) = \left[y_{1,1}(X_p, Z_p), \ldots, y_{1,N}(X_p, Z_p) \quad y_{2,1}(X_p, Z_p), \ldots, y_{N,N}(X_p, Z_p) \right]^{\mathrm{T}}. \tag{10}$$

We divide the detection area into grid areas in horizontal and vertical directions by GOB algorithm. Building a weight vector for any grid point (X, Z) is

$$\boldsymbol{w}(X, Z) = \boldsymbol{r}(X, Z), \tag{11}$$

where $\boldsymbol{r}(X, Z)$ is ralated to the relative phase shift that the signal at the grid point (X, Z) corresponds to in each array element.

$$\boldsymbol{r}(X, Z) = \left[r_{1,1}(X, Z), \ldots, r_{1,N}(X, Z) \quad r_{2,1}(X, Z), \ldots, r_{N,N}(X, Z) \right]^{\mathrm{T}}, \tag{12}$$

where

$$r_{n,m}(X, Z) = \exp\left\{ j2\pi(f_0 + (n-1)\Delta f) \cdot \left(- \frac{\sqrt{X^2 + Z^2 + ((n-1)d)^2 - 2(n-1)dX}}{v} - \frac{\sqrt{X^2 + Z^2 + ((m-1)d)^2 - 2(m-1)dX}}{v} \right) \right\}, \tag{13}$$

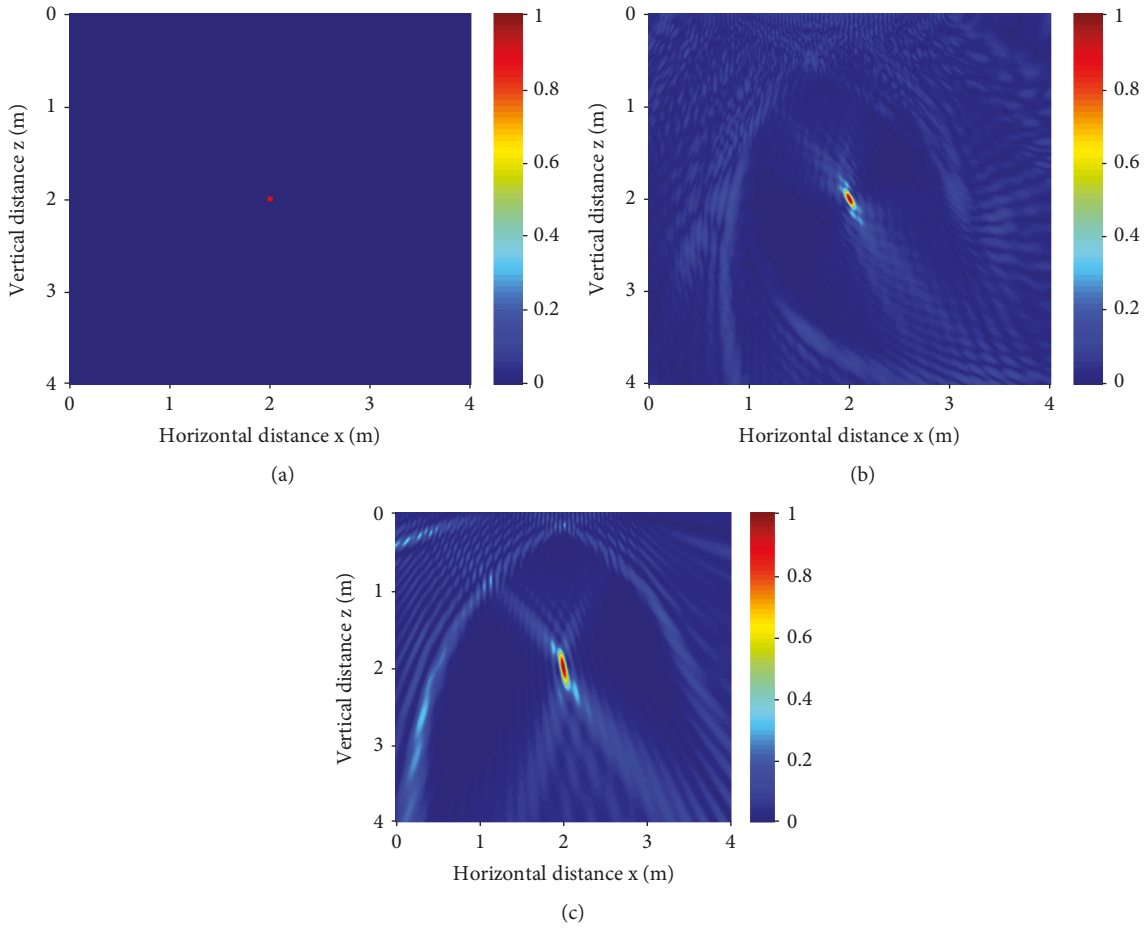

Figure 3: Single target detection: (a) actual position of target, (b) FDA-MIMO radar, and (c) conventional MIMO radar.

where X and Z are the horizontal and vertical distances between the grid point (X, Z) and the reference element, respectively.

We deal with the echo data through the weight vector constructed by (11). The output is as follows:

$$I(X,Z) = \left|\boldsymbol{w}^{\mathrm{H}}(X,Z)\mathbf{y}\right|, \tag{14}$$

where $I(X, Z)$ is the output value at the grid point (X, Z), $\boldsymbol{w}$ (X, Z) is the weight vector, and $\boldsymbol{y}$ is the vector representation of all echo data in (10).

The target detection in the region can be completed by traversing the whole detection space according to (14), and the detection result is displayed by the two-dimensional image.

Based on the above analysis, the steps of data processing and imaging display in this paper are summarized as follows:

Step 1. Demodulating the signals emitted by each transmitting element through the matched filters at the receiving end of the FDA-MIMO radar

Step 2. Expressing the demodulated echo data in vector form

Step 3. Dividing the detection area into grid areas in the horizontal and vertical directions and building a weight vector for any grid point by GOB algorithm

Step 4. Dealing with the echo data which is in vector form through the weight vector and calculating the pixel value at the current grid point

Step 5. Completing the target detection in the region by traversing the whole grid space and computing the pixel values at all grid points

4. Simulation and Analysis

In this section, experiments are implemented to validate the effectiveness of the proposed approach. In the simulations, we consider that the number of transmitting elements and receiving elements is both $N = 21$. The reference carrier frequency is $f_0 = 1$ GHz while the frequency increment of FDA-MIMO radar is $\Delta f = 0.02$ GHz. The element spacing is $d = 0.15$ m. The relative dielectric constant of the underground medium is $\varepsilon = 9$. The noise is zero-mean Gaussian white noise. SNR = 10 dB. The number of snapshots is $L = 100$.

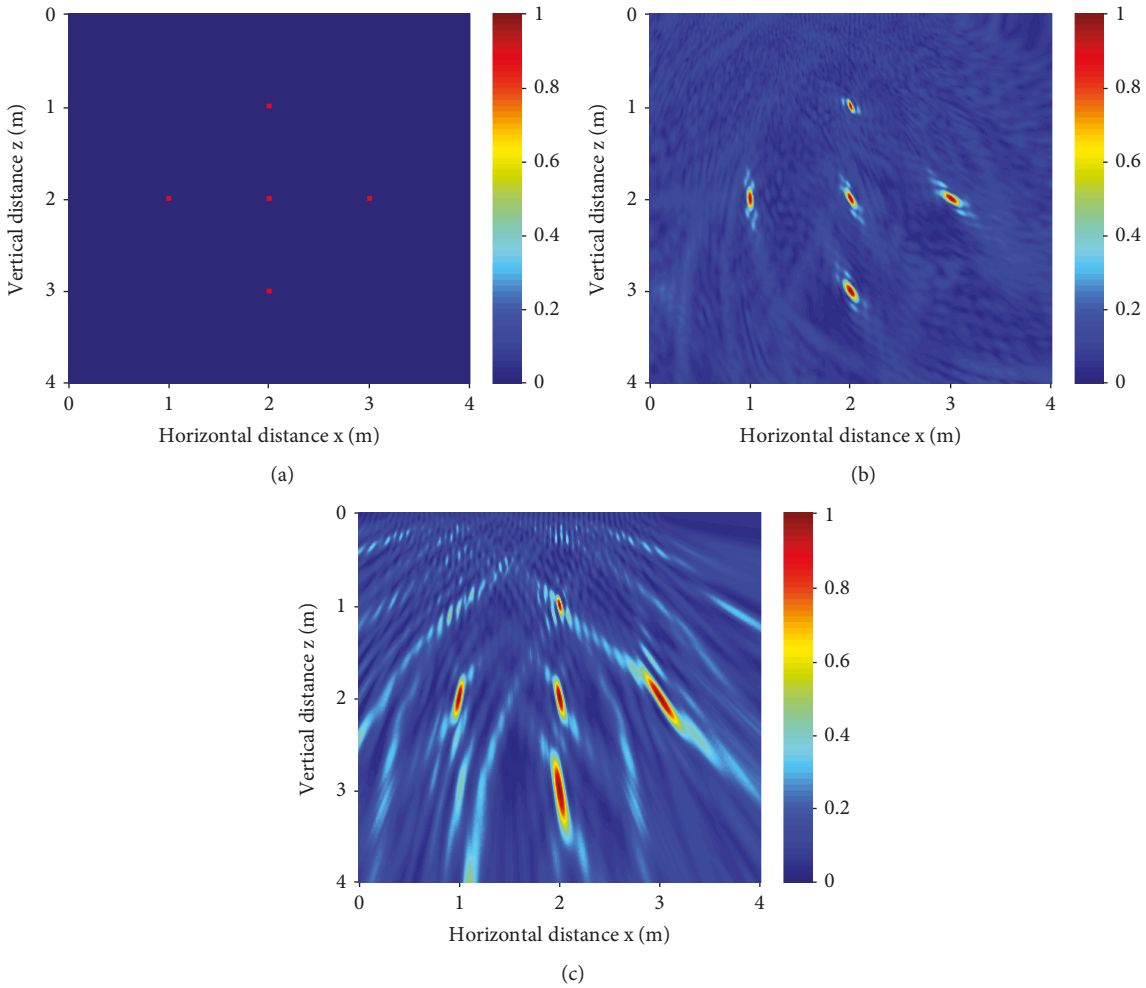

Figure 4: Multitargets detection: (a) actual position of targets, (b) FDA-MIMO radar, and (c) conventional MIMO radar.

4.1. Imaging Analysis

Experiment 1. We consider the situation of single target and set up one point target that the coordinate is (2 m, 2 m), as shown in Figure 3(a). It is assumed that the reflection coefficient of the target is 1. Figure 3(b) is the simulation result of FDA-MIMO radar. Figure 3(c) is the simulation result of conventional MIMO radar. We can see from the simulation results that both the FDA-MIMO radar and the conventional MIMO radar can locate the target. Compared with the detection result of conventional MIMO radar, the positioning effect of FDA-MIMO radar is more accurate and the interference of the pixel values from the nontarget area is smaller.

Experiment 2. We consider the situation of multitargets and set up five point targets that the coordinates are (1 m, 2 m), (2 m, 1 m), (2 m, 2 m), (2 m, 3 m), and (3 m, 2 m), respectively, as shown in Figure 4(a). It is assumed that the reflection coefficients of all targets are 1. Figure 4(b) is the simulation result of FDA-MIMO radar. Figure 4(c) is the simulation result of conventional MIMO radar. We can see from the simulation results that the detection of FDA-MIMO radar can clearly locate the five targets, and the pixel values of the nontarget region have little interference for us to judge the targets. Although the conventional MIMO radar can detect the approximate position of the targets, the positioning effect is not ideal from the simulation image. Compared with FDA-MIMO radar detection, conventional MIMO radar detection cannot achieve accurate positioning, and its interference of the pixel values from the nontarget area is great for us to judge the targets.

Experiment 3. We consider the situation of one strong target located at (1.5 m, 2 m) and one weak target located at (2.5 m, 2 m), as shown in Figure 5(a). It is assumed that the reflection coefficient of strong target is 1, and the reflection coefficient of weak target is 0.7. Figure 5(b) is the simulation result of FDA-MIMO radar. Figure 5(c) is the simulation result of conventional MIMO radar. We can see from the simulation results that the detection of FDA-MIMO radar can clearly distinguish two different energy targets. Compared with FDA-MIMO radar detection, conventional MIMO radar detection can still distinguish the two different energy targets due to the small number of targets, but its interference of the pixel values from the nontarget area still exists.

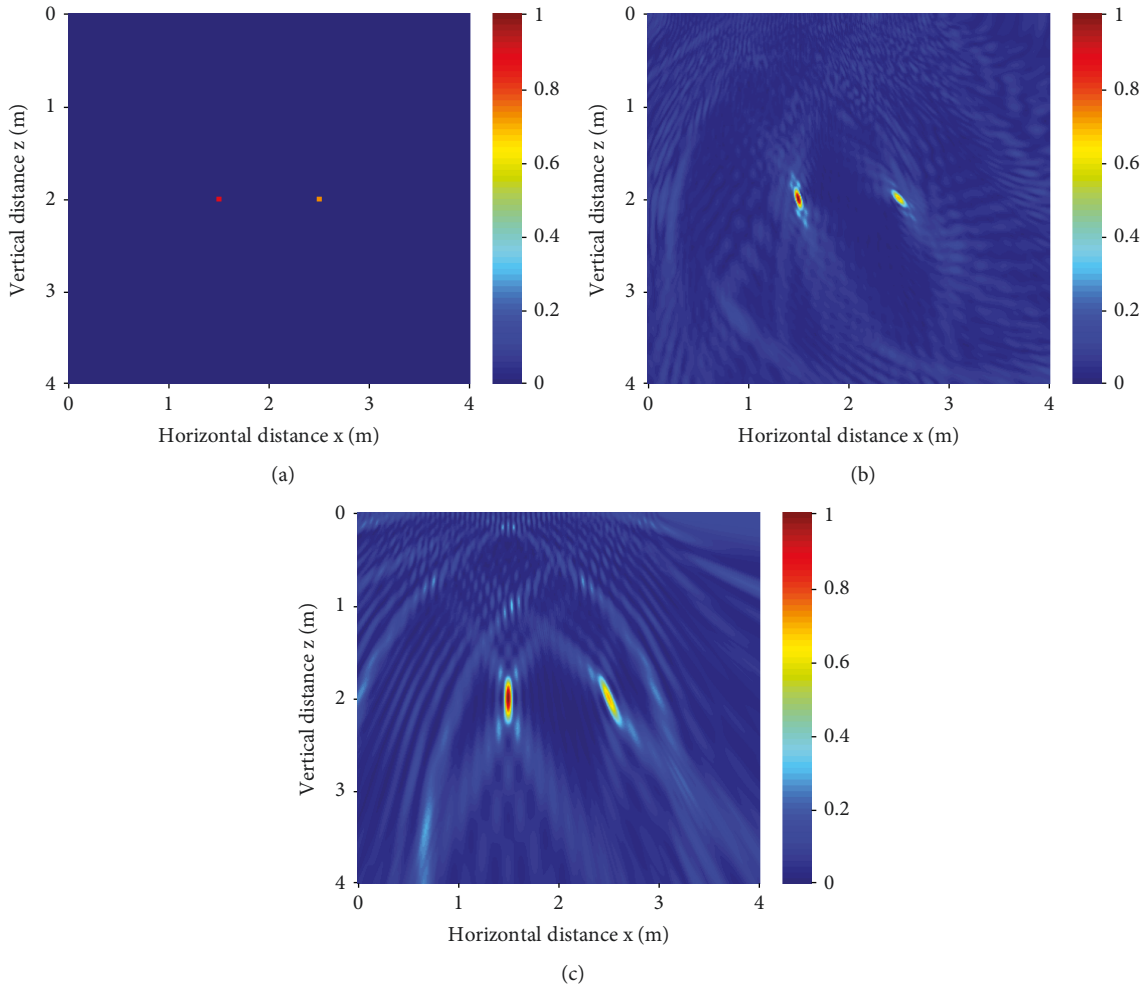

Figure 5: One strong target and one weak target detection: (a) actual position of targets, (b) FDA-MIMO radar, and (c) conventional MIMO radar.

Experiment 4. We consider the situation of two strong targets located at (2.5 m, 1.5 m) and (1.5 m, 2.5 m) and the two weak targets located at (1.5 m, 1.5 m) and (2.5 m, 2.5 m), as showed in Figure 6(a). It is assumed that the reflection coefficients of the strong targets are 1 and the reflection coefficients of the weak targets are 0.7. Figure 6(b) is the simulation result of FDA-MIMO radar. Figure 6(c) is the simulation result of conventional MIMO radar. We can see from the simulation results that the detection of FDA-MIMO radar can still accurately locate the four targets and can clearly distinguish the strong and weak targets, when the number of targets increases. While the positioning accuracy of conventional MIMO radar detection is obviously lower than that of FDA-MIMO radar detection, and it is not easy for us to determine the weak targets because of the large interference of the pixel values from the nontarget area. When the target number further increases or the reflection coefficient of the weak target is lower than the current one, it will be difficult for us to distinguish the weak targets in the image and it is easy to judge the false targets caused by the pixel values from the nontarget area into weak targets.

4.2. RMSE Analysis. In order to evaluate the results of the simulation more objectively, we introduce the root mean square error (RMSE) to judge the interference of the pixel values of the nontarget area in the image, which is defined as follows:

$$\mathrm{RMSE} = \sqrt{\frac{1}{K}\sum_{k=1}^{K}(I_r - I_i)^2}, \tag{15}$$

where K is the total number of pixels in the nontarget area, I_r is the actual pixel value of the kth pixel in the image, and I_i is the ideal pixel value of the kth pixel in the image. The greater the RMSE is, the greater the interference. The variation of the RMSE with the increase of observed targets is showed in Figure 7.

Experiment 5. Comparison between FDA-MIMO radar detection and conventional MIMO radar detection, when the number of snapshots is $L = 100$

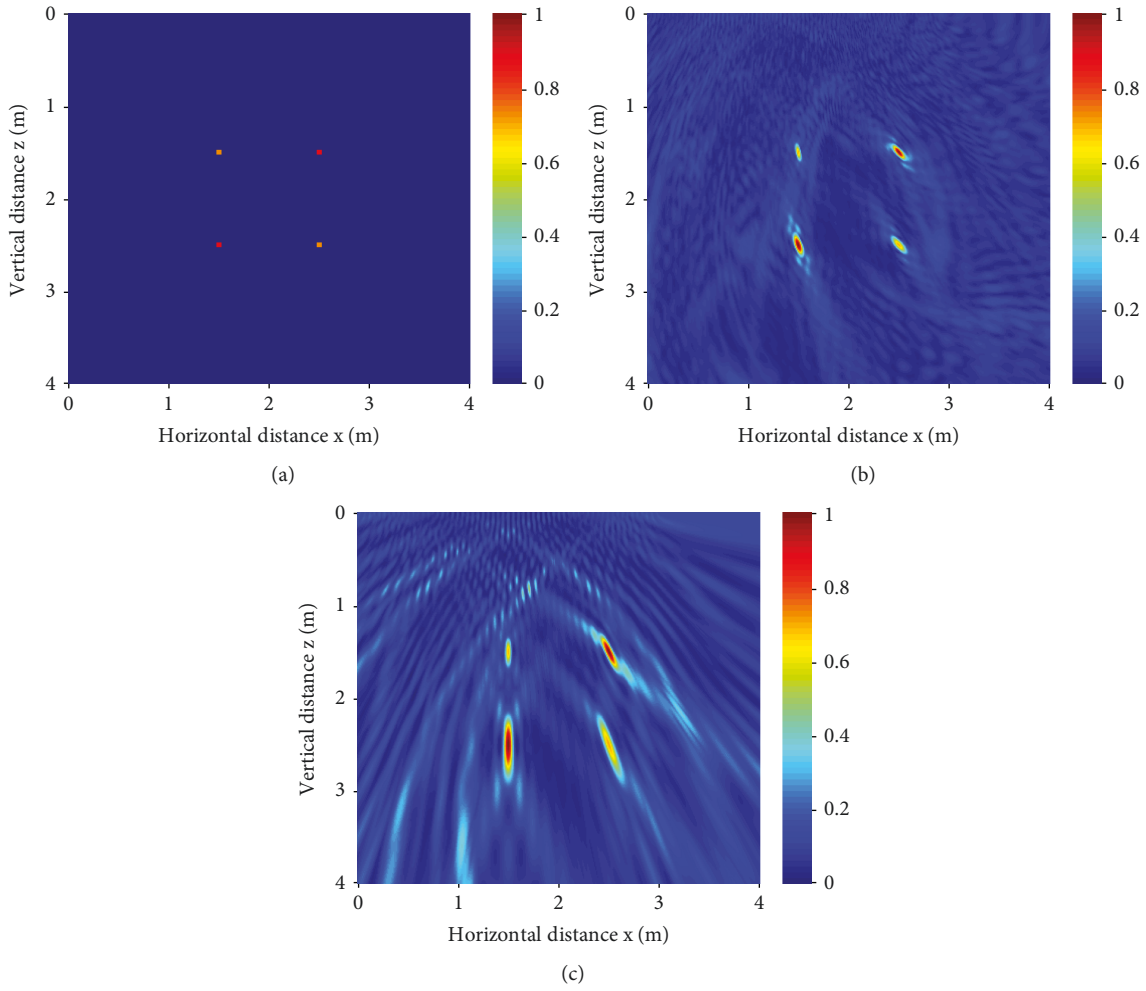

Figure 6: Two strong target and two weak target detection: (a) actual position of target, (b) FDA-MIMO radar, and (c) conventional MIMO radar.

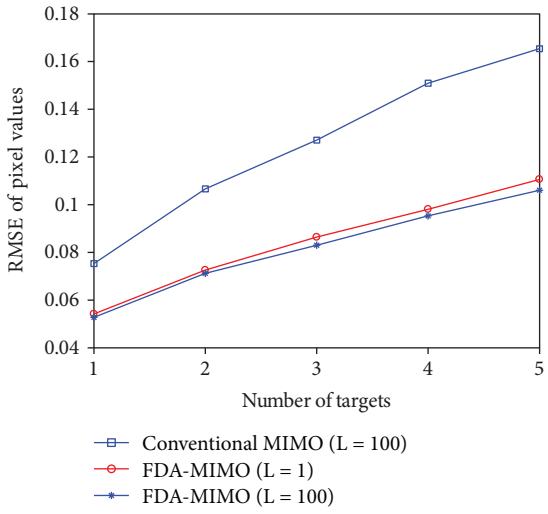

Figure 7: RMSE of pixel values in nontarget area.

We can see from Figure 7 that in the case of $L = 100$, the RMSE of the pixel values in the nontarget region detected by the FDA-MIMO radar is significantly lower than the RMSE detected by the conventional MIMO radar. With the increase of the number of observation targets, both the FDA-MIMO radar detection and the conventional MIMO radar detection have significantly increased the RMSE, and the increase detected by the conventional MIMO radar is greater. According to the above analysis, we can conclude that the detection results of FDA-MIMO radar are better than the detection results of conventional MIMO radar by using our detection method.

Experiment 6. The comparison of FDA-MIMO radar detection between the number of snapshots $L = 100$ and $L = 1$

We can see from Figure 7 that in the case of FDA-MIMO radar detection, the RMSE of $L = 1$ is very close to the RMSE of $L = 100$. It is only a little larger than the RMSE of $L = 100$ of the FDA-MIMO radar detection but far less than the RMSE of $L = 100$ of the conventional MIMO radar detection. It means that FDA-MIMO radar detection can achieve good detection results with single sampling by using the data processing method of this paper. In fact, in practical applications, judging the effect of detection is not only based on the detected image but also the time spent in the detection.

The time spent on data processing differs greatly between single sampling and 100 sampling, and time-consuming detection will limit its application in practice. Therefore, the advantage of good detection result that can be achieved by single sampling makes this method more conducive to engineering implementation.

5. Conclusion

In this paper, FDA-MIMO radar is applied to the detection of near-subsurface targets. Based on the analysis of the signal model, it is verified that the FDA-MIMO radar has a good detection effect for near-subsurface targets by GOB algorithm through theoretical simulation. Compared with conventional MIMO radar, the FDA-MIMO radar can get higher positioning accuracy through the analysis of 2D-images and the comparison of RMSE by using the proposed detection method.

Notations

$(\cdot)^{\mathrm{T}}$: Matrix transpose
$(\cdot)^{\mathrm{H}}$: Matrix conjugate transpose.

Data Availability

The data used to support the findings of this study are available from the corresponding author upon request.

Conflicts of Interest

The authors declare that they have no conflicts of interest.

Acknowledgments

This work was supported by the National Natural Science Foundation of China (grant numbers 61861011, 61461012 and 61871425), the Guangxi Natural Science Foundation (grant numbers 2016GXNSFAA380036 and 2018GXNSFAA138091), the Guangxi Key Laboratory of Wireless Wideband Communication and Signal Processing, the Guangxi Key Laboratory of Automatic Detection Technology and Instrument Foundation (grant number GXKL06160110), and the Science and Technology on Near-Surface Detection Laboratory Foundation (grant number TCGZ2017A010).

References

[1] V. R. N. Santos and F. L. Teixeira, "Application of time-reversal-based processing techniques to enhance detection of GPR targets," *Journal of Applied Geophysics*, vol. 146, pp. 80–94, 2017.

[2] F. Yang, X. Qiao, Y. Zhang, and X. Xu, "Prediction method of underground pipeline based on hyperbolic asymptote of GPR image," in *Proceedings of the 15th International Conference on Ground Penetrating Radar*, pp. 674–678, Brussels, Belgium, June 2014.

[3] V. R. N. Santos and F. L. Teixeira, "Study of time-reversal-based signal processing applied to polarimetric GPR detection of elongated targets," *Journal of Applied Geophysics*, vol. 139, pp. 257–268, 2017.

[4] Q. Hoarau, G. Ginolhac, A. M. Atto, and J. M. Nicolas, "Robust adaptive detection of buried pipes using GPR," *Signal Processing*, vol. 132, pp. 293–305, 2017.

[5] M. Jabbarian-Jahromi and M. H. Kahaei, "Two-dimensional SLIM with application to pulse Doppler MIMO radars," *EURASIP Journal on Advances in Signal Processing*, vol. 2015, no. 1, 2015.

[6] J. Liu, S. Zhou, W. Liu, J. Zheng, H. Liu, and J. Li, "Tunable adaptive detection in colocated MIMO radar," *IEEE Transactions on Signal Processing*, vol. 66, no. 4, pp. 1080–1092, 2018.

[7] P. Chen, L. Zheng, X. Wang, H. Li, and L. Wu, "Moving target detection using colocated MIMO radar on multiple distributed moving platforms," *IEEE Transactions on Signal Processing*, vol. 65, no. 17, pp. 4670–4683, 2017.

[8] G. U. Gen-Rui, "Parameter estimation with bistatic MIMO radar," *Information Technology*, vol. 2018, no. 1, 2018.

[9] J. Qian, Z. He, N. Huang, and B. Li, "Transmit designs for spectral coexistence of MIMO radar and MIMO communication system," *IEEE Transactions on Circuits and Systems II: Express Briefs*, no. 99, p. 1, 2018.

[10] P. Antonik, M. C. Wicks, H. D. Griffiths, and C. J. Baker, "Frequency diverse array radars," in *IEEE Conference on Radar*, p. 3, New York, NY, USA, 2006.

[11] M. C. Wicks and P. Antonik, *Frequency Diverse Array with Independent Modulation of Frequency, Amplitude, and Phase*, US, US7319427, 2008.

[12] J. Huang, K. F. Tong, and C. J. Baker, "Frequency diverse array with beam scanning feature," in *2008 IEEE Antennas and Propagation Society International Symposium*, pp. 1–4, San Diego, CA, USA, July 2008.

[13] J. Huang, K.-F. Tong, K. Woodbridge, and C. Baker, "Frequency diverse array: simulation and design," in *2009 IEEE Radar Conference*, pp. 1–4, Pasadena, CA, USA, 2009.

[14] P. Baizert, T. B. Hale, M. A. Temple, and M. C. Wicks, "Forward-looking radar GMTI benefits using a linear frequency diverse array," *Electronics Letters*, vol. 42, no. 22, pp. 1311-1312, 2006.

[15] J. Farooq, M. A. Temple, and M. A. Saville, "Application of frequency diverse arrays to synthetic aperture radar imaging," in *2007 International Conference on Electromagnetics in Advanced Applications*, pp. 447–449, Torino, Italy, September 2007.

[16] P. F. Sammartino, C. J. Baker, and H. D. Griffiths, "Range-angle dependent waveform," in *2010 IEEE Radar Conference*, pp. 511–515, Washington, DC, USA, 2010.

[17] L. Zhuang and X. Liu, "Application of frequency diversity to suppress grating lobes in coherent MIMO radar with separated subapertures," *EURASIP Journal on Advances in Signal Processing*, vol. 2009, no. 1, Article ID 481792, 2009.

[18] K. V. Shanbhag, D. Deb, and M. Kulkarni, "MIMO radar with spatial-frequency diversity for improved detection performance," in *2010 International Conference on Communication Control and Computing Technologies*, pp. 66–70, Ramanathapuram, India, October 2010.

[19] P. F. Sammartino, C. J. Baker, and H. D. Griffiths, "Frequency diverse MIMO techniques for radar," *IEEE Transactions on Aerospace and Electronic Systems*, vol. 49, no. 1, pp. 201–222, 2013.

[20] K. Gao, H. Shao, H. Chen, J. Cai, and W. Q. Wang, "Impact of frequency increment errors on frequency diverse array MIMO in adaptive beamforming and target localization," *Digital Signal Processing*, vol. 44, no. C, pp. 58–67, 2015.